

Correlations after Quantum Quenches in the XXZ Spin Chain: Failure of the Generalized Gibbs Ensemble

B. Pozsgay,¹ M. Mestyán,¹ M. A. Werner,² M. Kormos,¹ G. Zaránd,² and G. Takács^{1,*}

¹MTA-BME “Momentum” Statistical Field Theory Research Group

Department of Theoretical Physics, Budapest University of Technology and Economics, 1111 Budapest, Budafoki út 8, Hungary

²MTA-BME “Momentum” Exotic Quantum Phases Research Group

Department of Theoretical Physics, Budapest University of Technology and Economics, 1111 Budapest, Budafoki út 8, Hungary

We study the nonequilibrium time evolution of the spin-1/2 anisotropic Heisenberg (XXZ) spin chain, with a choice of dimer product and Néel states as initial states. We investigate numerically various short-ranged spin correlators in the long-time limit and find that they deviate significantly from predictions based on the generalized Gibbs ensemble (GGE) hypotheses. By computing the asymptotic spin correlators within the recently proposed quench-action formalism [Phys. Rev. Lett. 110, 257203 (2013)], however, we find excellent agreement with the numerical data. We, therefore, conclude that the GGE cannot give a complete description even of local observables, while the quench-action formalism correctly captures the steady state in this case.

PACS numbers: 02.30.Ik, 05.70.Ln, 75.10.Jm

Introduction.— Recent, spectacular advances in the field of ultracold atoms enabled experimentalists to investigate the coherent time evolution of almost perfectly isolated quantum many-body systems [1–4]. These new developments triggered tremendous theoretical interest [5–18] in a long-standing problem of fundamental physical importance: do isolated quantum systems reach an equilibrium in some sense, and if the answer is positive, what is the nature of the steady state reached?

In the absence of external driving forces, generic systems are expected to reach a steady state locally indistinguishable from thermal equilibrium [5, 7]. However, integrable systems behave differently because conservation of the expectation values of extra local charges prevents relaxation to a thermal state. It was suggested in Ref. [19] that in the integrable case the long-time asymptotic stationary state is described by a statistical ensemble involving all the local conserved charges $\{\hat{Q}_i\}$, the generalized Gibbs ensemble (GGE), defined by the density matrix

$$\hat{\rho}_{\text{GGE}} = \frac{1}{Z} e^{-\sum_i \beta_i \hat{Q}_i}, \quad Z = \text{Tr} e^{-\sum_i \beta_i \hat{Q}_i}, \quad (1)$$

where the “chemical potentials” $\{\beta_i\}$ are determined by the expectation values of the charges in the ensemble and the initial quantum state.

The GGE idea has by now become widely accepted in the field and has been verified in several specific cases. Until recently, however, most investigations concerning GGE were carried out in theories equivalent to free fermions [20–29] or by numerical studies of relatively small systems [30, 31]. It is only recently that it has become possible to examine genuinely interacting integrable systems such as the one-dimensional Bose gas [32–34], the XXZ Heisenberg spin chain [1, 2, 36] or field theories [38–40].

However, until now there have only been a few precision numerical tests for the predictions of the GGE

against real-time dynamics [1]. In our Letter, we perform real-time numerical simulations on a genuinely interacting quantum system, the anisotropic Heisenberg model, and compare the relaxation of various local spin-spin correlation functions to the predictions of two competing theories: the overlap-incorporating thermodynamic Bethe ansatz (OTBA) approach, which implements the quench-action method [41], and the widely accepted GGE.

In agreement with some recent observations [42, 43] we find that these two approaches yield markedly different predictions. We arrive at a surprising conclusion: while the numerical results agree spectacularly with the OTBA, they differ significantly from the exact predictions of the GGE in a number of cases (see Fig. 2). These results lead to the inevitable conclusion that the GGE approach fails as a generic description of steady states in genuinely interacting integrable quantum systems.

Quantum quench in the XXZ chain.— The XXZ Heisenberg chain is a chain of $s = 1/2$ spins interacting via the Hamiltonian

$$H = - \sum_{i=1}^L [\sigma_i^x \sigma_{i+1}^x + \sigma_i^y \sigma_{i+1}^y + \Delta (\sigma_i^z \sigma_{i+1}^z - 1)], \quad (2)$$

where $\sigma_i^{x,y,z}$ are the Pauli matrices at site i . This model describes magnetism in real compounds [44] and plays a fundamental role in the theory of strongly correlated condensed-matter systems [45]. Here we focus on the Ising regime $\Delta > 1$, which corresponds to a gapped antiferromagnetic phase in equilibrium.

We implement the nonequilibrium process via the paradigmatic setting of quantum quench [46, 47], whereby the time evolution of the system starts from the ground state of some Hamiltonian but then at time $t = 0$ some parameter of the system is abruptly changed. Quantum quenches of this kind can be implemented in a

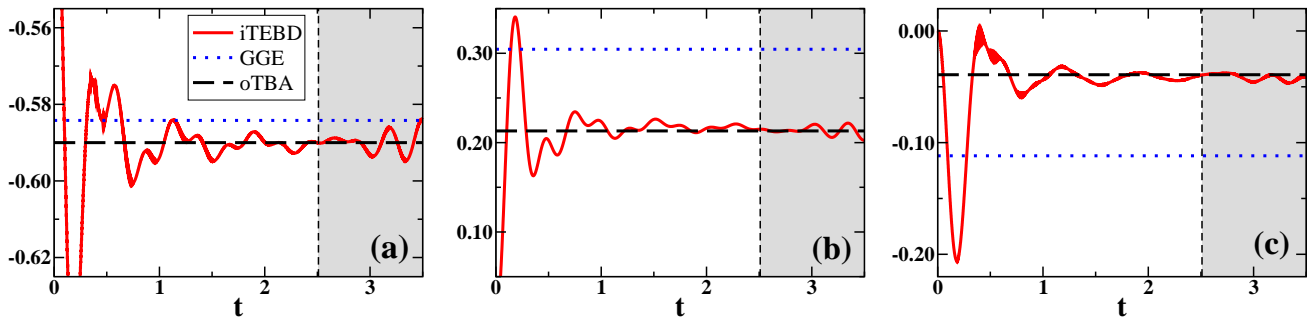


FIG. 1: Numerical simulation of the time evolution of correlation functions (a) $\langle\sigma_1^z\sigma_2^z\rangle$, (b) $\langle\sigma_1^z\sigma_3^z\rangle$, (c) $\langle\sigma_1^z\sigma_4^z\rangle$ starting from the dimer initial state (4) for anisotropy $\Delta = 4$ as obtained by ITEBD (red lines). In the shaded region the results are not reliable. The horizontal lines show the GGE prediction [1] (blue dotted lines) and the prediction of the overlap TBA of the quench-action approach (black dashed lines).

controlled fashion by realizing the XXZ chain in systems of cold atoms in optical lattices [48–52].

As initial states, we consider the translationally invariant projection of the Néel state

$$|\Psi_0^N\rangle = \frac{1 + \hat{T}}{\sqrt{2}} |\uparrow\downarrow\uparrow\dots\rangle = \frac{1}{\sqrt{2}} (|\uparrow\downarrow\uparrow\dots\rangle + |\downarrow\uparrow\downarrow\dots\rangle), \quad (3)$$

which is a ground state in the $\Delta \rightarrow \infty$ limit, and the similarly symmetrized dimer product state

$$|\Psi_0^D\rangle = \frac{1 + \hat{T}}{\sqrt{2}} \left| \frac{(\uparrow\downarrow - \downarrow\uparrow)}{\sqrt{2}} \frac{(\uparrow\downarrow - \downarrow\uparrow)}{\sqrt{2}} \dots \right\rangle, \quad (4)$$

which is one of the ground states of the Majumdar-Ghosh Hamiltonian [53]. Here, \hat{T} is the one site translation operator on the lattice. It is expected that ground states of local Hamiltonians always relax to a steady state.

Failure of the GGE description of the steady state correlations.— To demonstrate that the GGE cannot give an appropriate description of the steady state, we compare its predictions for correlation functions with the results of real-time out-of-equilibrium numerical simulations, performed using the infinite size time evolving block decimation (ITEBD) algorithm [54, 55]. In the simulations, translational invariance of the initial states in Eqs. (3) and (4) was implemented by averaging over the two components of the states [56]. The time evolution of three different correlators is shown in Fig. 1 for a quench starting from the dimer state for $\Delta = 4$ (red lines). The correlation functions quickly converge to stationary values before the simulations break down for large times (shaded regions) [57].

Strikingly, the exact GGE values of Ref. [1] (blue dotted lines in Fig. 1) deviate significantly from the ITEBD results. We report similar deviations for all $\Delta > 1$ in Fig. 2, where we display the long-time asymptotic values extracted from the ITEBD simulation (red circles) together with the GGE predictions (squares) for $\langle\sigma_1^z\sigma_2^z\rangle$ and $\langle\sigma_1^z\sigma_3^z\rangle$, as functions of Δ . We included truncated

GGE (TGGE) results [2, 36] as well, obtained by keeping the first six nonzero charges in the density matrix (1). The discrepancy between the GGE and the ITEBD results is evident (for additional numerical data, see the Supplemental Material [58]).

The mismatch between real-time simulations and GGE results could be, in principle, the result of long relaxation times beyond the reach of the ITEBD simulations. We rule out this possibility by applying an alternative theoretical method, the overlap thermodynamic Bethe ansatz (OTBA) which implements the quench-action approach [34, 41] (see below), and predicts *exactly* the asymptotic values of the correlations. These values, shown as black dashed lines in Fig. 1 and black stars in Fig. 2, are clearly in excellent agreement with our ITEBD results. The state predicted by the OTBA is a steady state of maximal conditional entropy. Therefore, the excellent agreement proves that the ITEBD simulation has reached the true asymptotic steady state, and, thus makes the evidence for the breakdown of the GGE conclusive. Moreover, it also demonstrates that the quench-action-approach-based OTBA indeed correctly captures the steady state of the XXZ model.

The TGGE predictions evaluated in Ref. [2] and the OTBA results are also different in the Néel case, but for large Δ , where the TGGE is reliable, this difference is beyond our numerical resolution (Supplemental Material [58]). We obtained similar results for x - x correlators for both initial states, although for the latter ITEBD is not as accurate as for the z - z correlators (cf. Ref. [59]).

We remark that translational invariance would be broken for the dimer state without the symmetrization under \hat{T} in Eqs. (3) and (4), and it is yet an open question whether it is restored in the long-time limit after the quench [1, 27]. Nevertheless, the GGE was expected to describe the average over the two components of the states (3) and (4), and yet it fails to do so. Note that for the observable $\langle\sigma_1^z\sigma_3^z\rangle$ translational averaging is immate-

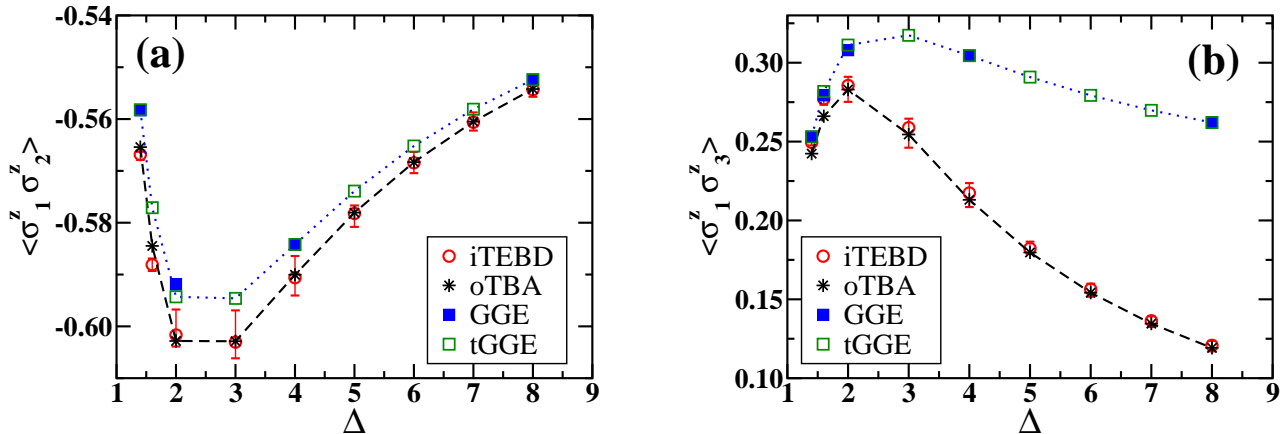


FIG. 2: Δ dependence of the ITEBD (red circles with error bars), overlap TBA (black stars), full GGE [1] (full blue squares) and truncated GGE (empty green squares) results for the large time expectation values (a) $\langle \sigma_1^z \sigma_2^z \rangle$ and (b) $\langle \sigma_1^z \sigma_3^z \rangle$ after the quench from the dimer initial state (4).

rial since it is identical on both sublattices.

Overlap thermodynamic Bethe ansatz (OTBA).—

The OTBA method is formulated in the framework of the Bethe ansatz (BA) [60], used to diagonalize the XXZ Hamiltonian (2). Eigenfunctions corresponding to spin waves of M flipped spins on a chain of length L are parametrized by a set of M complex numbers $\{\lambda_j\}$, called rapidities. Spin waves can form bound states described by specific configurations of rapidities, called strings [61]. In the thermodynamic limit (TDL), defined by $M \rightarrow \infty$, $L \rightarrow \infty$ with M/L fixed, it is convenient to introduce the densities $\rho_n(\lambda)$ of n strings in rapidity space, together with the densities $\rho_n^h(\lambda)$ of unoccupied levels (holes).

The quench-action approach of Ref. [41] has been developed to describe the steady state following a quantum quench in Bethe ansatz integrable systems and has been implemented before for the transverse field Ising chain [41] and the Lieb-Liniger model [34]. This variational approach selects the relevant states by minimizing the generalized free energy (quench action)

$$\mathcal{S}(\{\rho_n\}) = -\frac{2}{L} \text{Re} \ln \langle \Psi_0 | \{\rho_n(\lambda)\} \rangle - s(\{\rho_n(\lambda)\}). \quad (5)$$

The first term involves the overlap between the initial state $|\Psi_0\rangle$ and the steady state $|\{\rho_n(\lambda)\}\rangle$, characterized by the string densities $\{\rho_n(\lambda)\}$. The exact overlaps were computed for the Néel state (3) in Refs. [62–65]. Here we also generalized the overlap formula for the dimer product state (4) along the lines of Ref. [63]. In the TDL, the logarithm of both overlaps can be written as

$$-\frac{2}{L} \text{Re} \ln \langle \Psi_0 | \{\rho_n(\lambda)\} \rangle = \sum_{n=1}^{\infty} \int_{-\pi/2}^{\pi/2} d\lambda \rho_n(\lambda) g_n(\lambda) \quad (6)$$

with the $g_n(\lambda)$ functions given by

$$g_1^N(\lambda) = -\ln \frac{\tan(\lambda + \frac{i\eta}{2}) \tan(\lambda - \frac{i\eta}{2})}{4 \sin^2(2\lambda)}, \quad (7a)$$

$$g_1^D(\lambda) = -\ln \frac{\sinh^4(\eta/2) \cot^2(\lambda)}{\sin(2\lambda + i\eta) \sin(2\lambda - i\eta)} \quad (7b)$$

for the Néel and dimer states, respectively. In both cases $g_n^{N,D}(\lambda) = \sum_{j=1}^n g_1^{N,D}[\lambda + (i\eta/2)(n+1-2j)]$ for higher strings ($n > 1$).

The second term $s(\{\rho_n(\lambda)\})$ in Eq. (5) is the entropy density [61, 66] accounting for the number of microstates realizing the set of macroscopic $\{\rho_n(\lambda)\}$

$$s(\rho_n) = \sum_{n=1}^{\infty} \int d\lambda \frac{1}{2} \left[\rho_n \ln \frac{\rho_n + \rho_n^h}{\rho_n} + \rho_n^h \ln \frac{\rho_n + \rho_n^h}{\rho_n^h} \right]. \quad (8)$$

It is exactly half of the standard Yang-Yang entropy density [61, 66] due to the fact that only parity invariant microstates have nonzero overlap [34, 65].

The quench action (5) expresses the idea that the states relevant in the TDL are those with both large overlaps with the initial state and a large number of microscopic realizations. The steady state is captured by a saddle-point set of string densities, with the saddle-point approximation becoming exact in the TDL. The densities $\{\rho_n(\lambda)\}$ and $\{\rho_n^h(\lambda)\}$ are, however, not independent; interactions couple the rapidities of all the spin excitations, as expressed by the Bethe equations. As a consequence, the densities $\{\rho_n\}$ and $\{\rho_n^h\}$ satisfy coupled integral equations (constraints) [61]

$$a_n(\lambda) = \rho_n(\lambda) + \rho_n^h(\lambda) + \sum_{m=1}^{\infty} [T_{nm} \circ \rho_m](\lambda). \quad (9)$$

Here, $[a \circ b](\lambda) = \int_{-\pi/2}^{\pi/2} d\lambda' a(\lambda - \lambda') b(\lambda')$ denotes convolution, and the interaction kernel is expressed as $T_{nm} = (1 - \delta_{n,m}) a_{|n-m|} + a_{n+m} + 2 \sum_{j=1}^{\min\{n,m\}-1} a_{|n-m|+2j}$, with $\pi a_n(\lambda) = \sinh(n\eta) / [\cosh(n\eta) - \cos(2\lambda)]$ and $\cosh \eta = \Delta$. The constrained extremum of $\mathcal{S}(\{\rho_n(\lambda)\})$ is then found through the standard treatment [61] and leads to the following integral equations for the functions $\eta_n(\lambda) \equiv \rho_n^h(\lambda) / \rho_n(\lambda)$:

$$\ln \eta_n(\lambda) = g_n(\lambda) + \mu n + \sum_{m=1}^{\infty} [T_{nm} \circ \ln(1 + \eta_m^{-1})](\lambda). \quad (10)$$

Here, μ is a Lagrange multiplier introduced to fix the overall magnetization to zero. By examining the $g_n(\lambda)$, we obtained for both initial states that $\ln \eta_n \sim \eta n^2$ for large n . This implies that the higher strings are suppressed as $\propto e^{-\eta n^2}$, so the infinite set of equations (10) can be safely truncated to relatively few equations, and solved numerically. Having the numerical solution for η_n at hand, we can replace them into Eq. (9) and determine the densities efficiently. (For further technical details see Ref. [59]).

OTBA consistency checks. — There are several ways to check that the numerically obtained saddle-point string densities $\{\rho_n^*\}$ are, indeed, correct and correspond to the right initial states and to the right saddle point. A nontrivial check is provided by the computation of the norm of the initial state in the TDL, i.e.,

$$0 = -\frac{1}{L} \ln \langle \Psi_0 | \Psi_0 \rangle = \mathcal{S}(\{\rho_n^*(\lambda)\}), \quad (11)$$

with the quench action Eq. (5) evaluated via Eqs. (8) and (6) for the saddle-point solution. Equation (11) is, indeed, satisfied by our saddle-point solution within the accuracy of our numerical simulations $\mathcal{O}(10^{-8})$. Notice that if this integral sum rule was violated, then the spectral weight of the saddle-point solution would be zero in the TDL.

Another important consistency check is provided by the expectation values of the conserved charges. These can be expressed in terms of the saddle-point densities as [67]

$$\langle \hat{Q}_{2m} \rangle = \sum_{n=1}^{\infty} \int_{-\pi/2}^{\pi/2} d\lambda \rho_n^*(\lambda) q_n^{(2m)}(\lambda), \quad (12)$$

with $q_n^{(2m)}(\lambda) = 2\pi \sum_{j=1}^n [-(\partial/\partial\lambda)]^{2m} a_1[\lambda + (i\eta/2)(n+1-2j)]$, the energy, in particular, being given by $E = 2 \sinh \eta \langle \hat{Q}_2 \rangle$. The saddle-point values of these charges must equal their values in the initial states. These latter were computed for the symmetric Néel state in Refs. [2, 36]. Here we determined them using both these methods in the symmetrized dimer state, $|\Psi_0^D\rangle$. We evaluated the first six nonzero charges, $\{\langle \hat{Q}_{2m} \rangle\}_{m=1,\dots,6}$ and compared them with the expectation values computed from Eq. (12). Excellent agreement up to more than 8 digits is found in all cases, providing a further stringent verification of the OTBA solution.

Steady state correlations. — With the saddle-point string densities at hand, we then computed various short distance correlation functions in the steady state by making use of the recent results of two of the present authors, who provided exact formulas for the 2-point correlation functions in terms of the string densities [68]. We compared these values with the results of our ITEBD simulations. Excellent agreement is found between OTBA and ITEBD for both initial states and for all $\Delta > 1$ values (cf. Figs. 1 and 2 and the Supplemental Material [58] for detailed numerical data). This establishes the quench-action-approach-based OTBA as a correct description of the steady state and the failure of GGE at the same time.

Discussion. — In this Letter, we studied various correlation functions in the asymptotic steady states for quantum quenches in the XXZ spin chain. We found that the predictions of the generalized Gibbs ensemble differ significantly from the results of real-time ITEBD simulations in the dimer case, thereby signaling the breakdown of the GGE. We also determined these asymptotic correlators by applying the quench-action-based overlap TBA description of the steady state, and obtained numerically accurate predictions. We found that while the quench-action-based OTBA correctly captures the asymptotic steady state, the GGE fails for the states considered here. Finding a macroscopic statistical ensemble description of the steady state and clarifying the conditions for the validity of the GGE in strongly interacting systems, therefore, remain intriguing open questions.

Acknowledgments. — We would like to thank F. Pollmann and P. Moca for numerous discussions, their valuable feedback and the help they gave us to set up the TEBD calculations. M.K. is grateful to J.-S. Caux, J. De Nardis, and B. Wouters for useful discussions on some aspects of their work. M.K. acknowledges financial support from the Marie Curie IIF Grant No. PIIF-GA-2012-330076. M.A.W. and G.Z. acknowledge financial support from Hungarian Grants No. K105149 and CNK80991.

Note added. — During the final stages of this work, a related paper appeared [43] that independently arrived at Eq. (7a) and in which the difference between the GGE and the OTBA predictions for nearest-neighbor correlators in the quench starting from the Néel state was observed as well.

* Corresponding author, takacsg@eik.bme.hu

- [1] T. Kinoshita, T. Wenger, and D. S. Weiss, Nature (London) **440**, 900 (2006).
- [2] M. Cheneau, P. Barmettler, D. Poletti, M. Endres, P. Schauss, T. Fukuhara, C. Gross, I. Bloch, C. Kollath, and S. Kuhr, Nature (London) **481**, 484 (2012).
- [3] S. Trotzky, Y.-A. Chen, A. Flesch, I. P. McCulloch, U. Schollwck, J. Eisert, and I. Bloch, Nat. Phys. **8**, 325 (2012).

- [4] T. Fukuhara, P. Schau, M. Endres, S. Hild, M. Cheneau, I. Bloch, and C. Gross, *Nature (London)* **502**, 76 (2013).
- [5] A. Polkovnikov, K. Sengupta, A. Silva, and M. Vengalattore, *Rev. Mod. Phys.* **83**, 863 (2011).
- [6] C. Kollath, A. M. Läuchli, and E. Altman, *Phys. Rev. Lett.* **98**, 180601 (2007).
- [7] M. Rigol, V. Dunjko, and M. Olshanii, *Nature (London)* **452**, 854 (2008).
- [8] T. Barthel and U. Schollwöck, *Phys. Rev. Lett.* **100**, 100601 (2008).
- [9] M. Rigol, *Phys. Rev. Lett.* **103**, 100403 (2009).
- [10] M. Cramer and J. Eisert, *New J. Phys.* **12**, 055020 (2010).
- [11] L. F. Santos and M. Rigol, *Phys. Rev. E* **81**, 036206 (2010).
- [12] P. Barmettler, M. Punk, V. Gritsev, E. Demler, and E. Altman, *New J. Phys.* **12**, 055017 (2010).
- [13] M. C. Bañuls, J. I. Cirac, and M. B. Hastings, *Phys. Rev. Lett.* **106**, 050405 (2011).
- [14] P. Calabrese, F. H. L. Essler, and M. Fagotti, *Phys. Rev. Lett.* **106**, 227203 (2011).
- [15] P. Calabrese, F. H. L. Essler, and M. Fagotti, *J. Stat. Mech.* (2012) P07016.
- [16] N. Sedlmayr, J. Ren, F. Gebhard, and J. Sirker, *Phys. Rev. Lett.* **110**, 100406 (2013).
- [17] M. Marcuzzi, J. Marino, A. Gambassi, and A. Silva, *Phys. Rev. Lett.* **111**, 197203 (2013).
- [18] D. Iyer, H. Guan, and N. Andrei, *Phys. Rev. A* **87**, 053628 (2013).
- [19] M. Rigol, V. Dunjko, V. Yurovsky, and M. Olshanii, *Phys. Rev. Lett.* **98**, 050405 (2007).
- [20] M. A. Cazalilla, *Phys. Rev. Lett.* **97**, 156403 (2006).
- [21] D. Rossini, A. Silva, G. Mussardo, and G. E. Santoro, *Phys. Rev. Lett.* **102**, 127204 (2009).
- [22] P. Calabrese, F. H. L. Essler, and M. Fagotti, *J. Stat. Mech.* (2012) P07022.
- [23] M. A. Cazalilla, A. Iucci, and M.-C. Chung, *Phys. Rev. E* **85**, 011133 (2012).
- [24] V. Gurarie, *J. Stat. Mech.* P02014 (2013).
- [25] M. Fagotti and F. H. L. Essler, *Phys. Rev. B* **87**, 245107 (2013).
- [26] M. Collura, S. Sotiriadis, and P. Calabrese, *Phys. Rev. Lett.* **110**, 245301 (2013).
- [27] M. Fagotti, *J. Stat. Mech.* P03016 (2014).
- [28] M. Kormos, M. Collura, and P. Calabrese, *Phys. Rev. A* **89**, 013609 (2014).
- [29] S. Sotiriadis and P. Calabrese, *J. Stat. Mech.* (2014) P07024.
- [30] A. C. Cassidy, C. W. Clark, and M. Rigol, *Phys. Rev. Lett.* **106**, 140405 (2011).
- [31] T. M. Wright, M. Rigol, M. J. Davis, and K. V. Kheruntsyan, *Phys. Rev. Lett.* **113**, 050601 (2014).
- [32] J.-S. Caux and R. M. Konik, *Phys. Rev. Lett.* **109**, 175301 (2012).
- [33] M. Kormos, A. Shashi, Y.-Z. Chou, J.-S. Caux, and A. Imambekov, *Phys. Rev. B* **88**, 205131 (2013).
- [34] J. De Nardis, B. Wouters, M. Brockmann, and J.-S. Caux, *Phys. Rev. A* **89**, 033601 (2014).
- [35] B. Pozsgay, *J. Stat. Mech.* (2013) P07003.
- [36] M. Fagotti and F. H. L. Essler, *J. Stat. Mech.* (2013) P07012.
- [37] M. Fagotti, M. Collura, F. H. L. Essler, and P. Calabrese, *Phys. Rev. B* **89**, 125101 (2014).
- [38] D. Fioretto and G. Mussardo, *New J. Phys.* **12**, 055015 (2010).
- [39] G. Mussardo, *Phys. Rev. Lett.* **111**, 100401 (2013).
- [40] S. Sotiriadis, G. Takács, and G. Mussardo, *Phys. Lett. B* **734**, 52 (2014).
- [41] J.-S. Caux and F. H. L. Essler, *Phys. Rev. Lett.* **110**, 257203 (2013).
- [42] J.-S. Caux, in *Proceedings of the Workshop on Emergent Phenomena in the Dynamics of Quantum Matter, New York, 2014* (unpublished).
- [43] B. Wouters, M. Brockmann, J. De Nardis, D. Fioretto, M. Rigol, and J.-S. Caux, *Phys. Rev. Lett.* **113**, 117202 (2014).
- [44] A. Auerbach, *Interacting Electrons and Quantum Magnetism* (Springer, New York, 1994).
- [45] F. H. L. Essler and R. M. Konik, in *From Fields to Strings: Circumnavigating Theoretical Physics*, edited by Misha Shifman, Arkady Vainshtein, and John Wheeler, Ian Kogan Memorial Collection Vol. 3 (World Scientific, Singapore, 2004), p. 684.
- [46] P. Calabrese and J. Cardy, *J. Stat. Mech.* (2005) P04010.
- [47] P. Calabrese and J. Cardy, *Phys. Rev. Lett.* **96**, 136801 (2006).
- [48] A. B. Kuklov and B. V. Svistunov, *Phys. Rev. Lett.* **90**, 100401 (2003).
- [49] L.-M. Duan, E. Demler, and M. D. Lukin, *Phys. Rev. Lett.* **91**, 090402 (2003).
- [50] T. Barthel, C. Kasztelan, I. P. McCulloch, and U. Schollwöck, *Phys. Rev. A* **79**, 053627 (2009).
- [51] J. Simon, W. S. Bakr, R. Ma, M. E. Tai, P. M. Preiss, and M. Greiner, *Nature (London)* **472**, 307 (2011).
- [52] Y.-A. Chen, S. Nascimbène, M. Aidelsburger, M. Atala, S. Trotzky, and I. Bloch, *Phys. Rev. Lett.* **107**, 210405 (2011).
- [53] C. K. Majumdar and D. K. Ghosh, *J. Math. Phys.* **10**, 1388 (1969).
- [54] G. Vidal, *Phys. Rev. Lett.* **93**, 040502 (2004).
- [55] G. Vidal, *Phys. Rev. Lett.* **98**, 070201 (2007).
- [56] This approach is justified in the TDL, where off-diagonal contributions vanish.
- [57] The region of validity of the ITEBD simulations was determined by comparing results using different bond dimensions and the observed saturation of the entanglement. Our real-time simulation results are consistent with those obtained in Ref. [1].
- [58] See the Supplemental Material below for details of the ITEBD simulation and numerical data.
- [59] B. Pozsgay, M. Mestyán, M. A. Werner, M. Kormos, and G. Takács (to be published).
- [60] H. Bethe, *Zeitschrift für Physik* **71**, 205 (1931).
- [61] M. Takahashi, *Thermodynamics of One-Dimensional Solvable Models* (Cambridge University Press, Cambridge, England, 1999).
- [62] K. K. Kozłowski and B. Pozsgay, *J. Stat. Mech.* (2012) P05021.
- [63] B. Pozsgay, *J. Stat. Mech.* (2014) P06011.
- [64] M. Brockmann, J. De Nardis, B. Wouters, and J.-S. Caux, *J. Phys. A* **47**, 145003 (2014).
- [65] M. Brockmann, J. De Nardis, B. Wouters, and J.-S. Caux, arXiv:1403.7469.
- [66] C. N. Yang and C. P. Yang, *J. Math. Phys.* **10**, 1115 (1969).
- [67] M. Lüscher, *Nucl. Phys. B* **117**, 475 (1976).
- [68] M. Mestyán and B. Pozsgay, *J. Stat. Mech.* (2014) P09020.

Supplementary Material for EPAPS

Correlations after a quantum quench in the XXZ spin chain: failure of the generalized Gibbs ensemble

Numerical methods

In this section we present a collection of high precision numerical data as well as some details on the numerical simulations.

ITEBD simulation.— We performed the simulations by an ITEBD-code, which made use of the $U(1)$ rotational symmetry of the XXZ model around the z -axis. Maximal bond dimensions of the $U(1)$ blocks were set to $\chi_{\text{block}} = 400$, resulting in a total bond dimension $\chi_{\text{tot}} > 1000$. We used a first order Trotter-expansion for the time evolution operator with a time step $dt = 0.001$, and verified that decreasing this time step does not modify our results.

To control the reliability of our data, we computed the truncated weight at each time-step, and requested that the one-step truncated weight be less than 10^{-8} . As an alternative method, we ran the code with different bond dimensions and determined the time, where the results deviated upon increasing bond dimension. The two methods resulted in approximately the same threshold time. The error bars in Fig. 2 of the main text and Tables S1 and S2 below were then estimated by extracting the minimal and maximal values of the correlators before the threshold time in the last time interval of length 1.0.

For $\Delta = 1.4$ and $\Delta = 1.6$ it is difficult to estimate the error because for the times the simulation can reach there is still a drift of the correlation functions; in these cases the errors shown in the tables are computed from the fluctuations around this drifting average. The remaining drift of the average introduces a further systematical error, which is not included in our statistical estimate, and is hard to quantify reliably.

Precision of the OTBA solution.— The precision of the solution of the OTBA system was improved by extrapolation in the discretization used in the numerical solutions of the integral equations.

Checking the sum rule (11) by plugging in our numerical solution for different values of Δ for both initial states we found that while both the overlap (6) and the entropy (8) are of order $\mathcal{O}(10^{-1})$, their difference, i.e. the quench action (5) is of order $\mathcal{O}(10^{-8})$ and shrinks while increasing the number of equations included, therefore it is interpreted as a numerical error of the truncated OTBA system. This provides very strong evidence that we indeed found the correct saddle point solution.

Results.— The estimates of the asymptotic values of the correlations together with the OTBA predictions are listed for various Δ values in Table S1 for the zero momentum Néel state and in Table S2 for the dimer initial states. Based on the accuracy of the saturation of the sum rule and of the mean values of conserved charges, we can trust the results of the OTBA at least up to 7 digits. The tables also show the TGGE predictions and, when available from [1], the predictions of the full GGE as well.

In the Néel case the difference between the OTBA and TGGE results [2] is smaller than the accuracy of the ITEBD, except for $\Delta = 2$ where the TGGE seems to fail. However, in this case the TGGE with 6 charges has not yet converged in the truncation level. We expect that in the Néel case only the quenches to $\Delta < 1$ can conclusively decide between the OTBA and GGE predictions.

* Corresponding author, takacsg@eik.bme.hu

[1] M. Fagotti, M. Collura, F. H. L. Essler, and P. Calabrese, Phys. Rev. B **89**, 125101 (2014).

[2] B. Pozsgay, J. Stat. Mech. P07003 (2013).

	$\langle \sigma_1^z \sigma_2^z \rangle$	$\langle \sigma_1^z \sigma_3^z \rangle$	$\langle \sigma_1^z \sigma_4^z \rangle$
$\Delta = 2$, ITEBD	-0.6623(37)	0.3963(68)	-0.2967(50)
OTBA	-0.6602541	0.3929011	-0.2921120
TGGE	-0.648906	0.386578	-0.280383
$\Delta = 3$, ITEBD	-0.8145(28)	0.6493(52)	-0.5763(45)
OTBA	-0.8151215	0.6480874	-0.5745134
TGGE	-0.8140907	0.6501061	-0.5757850
$\Delta = 4$, ITEBD	-0.8875(18)	0.7815(34)	-0.7321(33)
OTBA	-0.8875741	0.7812765	-0.7317703
TGGE	-0.8874100	0.7824718	-0.7328197
$\Delta = 5$, ITEBD	-0.9254(9)	0.8537(16)	-0.8193(16)
OTBA	-0.9253052	0.8532200	-0.8187737
TGGE	-0.9252648	0.8538195	-0.8193336

TABLE S1: Correlation functions in the steady state computed from the real time ITEBD simulation starting from the Néel state, compared with the OTBA and TGGE predictions.

	$\langle \sigma_1^z \sigma_2^z \rangle$	$\langle \sigma_1^z \sigma_3^z \rangle$	$\langle \sigma_1^z \sigma_4^z \rangle$
$\Delta = 1.4$, ITEBD	-0.5668(8)	0.2495(16)	-0.1468(8)
OTBA	-0.5654103	0.2423652	-0.1399874
GGE	-0.5583	0.2531	-0.1428
TGGE	-0.5582489	0.2530204	-0.1426594
$\Delta = 1.6$, ITEBD	-0.5881(14)	0.2771(35)	-0.1640(27)
OTBA	-0.5844820	0.2660954	-0.1523768
GGE	-0.5751	0.2793	-0.1575
TGGE	-0.5771005	0.2818048	-0.1607061
$\Delta = 2$, ITEBD	-0.6017(36)	0.2856(79)	-0.1493(61)
OTBA	-0.6028190	0.2830639	-0.1483621
GGE	-0.5919	0.3080	-0.1653
TGGE	-0.5943014	0.3112498	-0.1694210
$\Delta = 3$, ITEBD	-0.6030(46)	0.2588(92)	-0.0922(75)
OTBA	-0.6028720	0.2545210	-0.0896056
TGGE	-0.5945574	0.3173677	-0.1409851
$\Delta = 4$, ITEBD	-0.5906(38)	0.2174(76)	-0.0421(56)
OTBA	-0.5900476	0.2130988	-0.0391867
GGE	-0.5842	0.3045	-0.1118
TGGE	-0.5841759	0.3045031	-0.1117982
$\Delta = 5$, ITEBD	-0.5782(21)	0.1823(38)	-0.0062(30)
OTBA	-0.5780574	0.1796867	-0.0048808
TGGE	-0.5739028	0.2908932	-0.0900247
$\Delta = 6$, ITEBD	-0.5684(21)	0.1564(41)	0.0175(34)
OTBA	-0.5683073	0.1541999	0.0187079
TGGE	-0.5652571	0.2793170	-0.0740645
$\Delta = 7$, ITEBD	-0.5606(18)	0.1364(34)	0.0345(29)
OTBA	-0.5605040	0.1345920	0.0355613
TGGE	-0.5581836	0.2698481	-0.0621113
$\Delta = 8$, ITEBD	-0.5543(16)	0.1208(33)	0.0473(26)
OTBA	-0.5542031	0.1191975	0.0480651
GGE	-0.5524	0.2621	-0.05291
TGGE	-0.5523842	0.2621091	-0.0529131

TABLE S2: Correlation functions in the steady state computed from the real time ITEBD simulation starting from the dimer state, compared with the OTBA, TGGE and GGE predictions.